DOR: 20.1001.1.2322388.2021.9.2.1.9

Research Paper

Cerium Oxide Nanoparticles as an Accelerating Agent for Zinc Phosphate Coatings with Enhanced Corrosion Resistance

Mohammad-Mehdi Akbari, Behrooz Shayegh Boroujeny*, Mehdi Raeissi

Department of Engineering, Shahrekord University, Shahrekord, Iran

ARTICLE INFO

Article history:

Received 29 July 2020
Accepted 11 August 2020
Available online 1 May 2021

Keywords:
Zinc phosphate coating
Ceria nanoparticle
Phosphating bath accelerator
Phosphate coating morphology
Corrosion behavior study

ABSTRACT

Cerium oxide (ceria, CeO_2) is a biocompatible ceramic oxide with a wide range of applications as catalysts, fuel cell systems, and sensors. In the present study, CeO_2 NPs were added to a zinc phosphate bath as an accelerator. The microstructural, morphological, and phase studies of coatings formed in the phosphating bath with and without CeO_2 NPs, were performed by scanning electron microscopy (SEM), field emission-SEM (FE-SEM), and X-ray diffraction spectroscopy (EDS). Besides, the corrosion behavior of phosphate coatings containing 0, 0.04, 0.07, and 0.1 g/L of CeO_2 NPs was evaluated using the Tafel polarization method and electrochemical impedance spectroscopy (EIS). The results showed significant differences in the microstructure, roughness, and phase structure of phosphate coatings with and without CeO_2 NPs. The optimum addition of CeO_2 NPs to the phosphating bath was equal to 0.07 g/L, in which, as compared to typical phosphate coating, the coating weight increased from 0.51 to 1.73 mg/cm^2 while the corrosion current density decreased from 12.5 to 2.2 µA/cm^2. Furthermore, the coating porosity decreased from 13.9 to 1.7 percent due to creating a denser coating with much better coverage by CeO_2 NPs.

* Corresponding Author . Tel.: +98 912 427 7420; fax: +98 3832324438
E-mail address: b.shayegh@eng.sku.ac.ir

1. Introduction

Metallic materials, particularly steels, are widely used in industries given their favorable mechanical properties, such as high strength, acceptable toughness, and ability to be recycled, and low cost. Nevertheless, the low corrosion resistance of these steels has limited their application [1, 2]. A variety of protective methods have been used to improve the corrosion resistance of carbon steels, and the application of phosphate coatings could be one of them. The phosphating method, which has a high degree of credibility and a long history of different industrial applications [3], is used not only to increase the corrosion resistance of carbon steels [4] but also to enhance the adhesion of the top organic coating, which is of great interest in industrial applications [5]. Besides corrosion protection and increasing color adhesion, phosphate coatings are also used for other purposes, such as metal forming, deep-drawing, and cold forging processes in which high-level deformation is produced [6-9]. In these applications, a phosphate coating can inhibit contact between the tool and the metal surfaces and does not have the lubricating properties itself but acts only as a separating layer and lubricant carrier [10, 11]. Iron, zinc, and manganese can be mentioned as some phosphate-containing solutions [12-14]. Meanwhile, because of providing superior corrosion resistance capability than the others, zinc phosphating is recognized as one of the most common methods for surface preparation [15, 16].

The traditional phosphating process is a time-consuming treatment and often acts under relatively high temperatures such as 90-98 ºC [17]. These disadvantages have caused the traditional phosphating process to account for enormous energy consumption. For solving the mentioned problems, the additive agents named accelerators are generally added to the phosphating baths for speeding up and lowering the operating temperature [18]. During the phosphating process, the metal surface is corroded in a phosphate solution, metal ions are released in the micro-anodic regions, and the hydrogen cations are reduced in micro-cathodic regions. Because of the accumulation of hydrogen atoms in cathodic regions, the reaction speed decreases. An excellent accelerator must react with hydrogen atoms to increase the reaction rate [19]. Traditional accelerators, such as nitrites, nitrates, and chlorates, have been used for this purpose. These accelerators can effectively improve the performance of the process but are harmful, and their use has recently been prohibited due to environmental pollution [20, 21].

Nowadays, the use of N.P.s as environment-friendly accelerators instead of the toxic accelerator agents in the phosphating process has gained considerable attention from a few researchers [19, 22-24]. In this regard, Sheng et al. [19] and later Jiang et al. [22] reviewed the accelerating effects of silicon dioxide N.P.s added to phosphating baths and suggested that nano-SiO_2 is helpful for phosphate nucleation and leads to smaller crystals. The authors concluded that the addition of SiO_2 NPs could control crystal size and is propitious to form new crystal nucleation and eliminate the defects by altering the content of growth orientations in the crystal phosphate. On the other hand, Shibli and Chacko [25] used TiO_2 NPs to create a TiO_2-incorporated phosphate coating on the galvanized steel surface. Their research results have revealed much better performance for the TiO_2-phosphate composite coating against corrosion attacks. Moreover, the authors proposed that the addition of titanium oxide N.P.s to the phosphating solution could activate a process to achieve the desired coating weight in a shorter period. Based on their opinions, nano-TiO_2 was responsible for the initial decrease of the potential, which is probably related to the surface activation of substrate dissolution occurring simultaneously with hydrogen evaluation reaction.

Cerium oxide (ceria, CeO_2) is one of the most widely used biocompatible ceramic oxides [26], with a wide range of applications as catalysts and as fuel cell systems in medical engineering and medicine [27-30]. It has been reported that the addition of CeO_2 NPs can improve the corrosion resistance and the microstructure of the coatings obtained from various coating methods, such as electroplated coatings [31], electroless deposited coatings [32, 33], and organic coatings [34]. However, there are a few reports about the use of CeO_2 NPs as the phosphating process accelerators. Therefore, given that no systematic review has been conducted on the use of CeO_2 NPs as additives in phosphating solutions, in the present study, the replacement of the traditional nitrite agent by non-toxic CeO_2 NPs as the environment-friendly accelerators was investigated. The morphology, composition and crystal structure, and corrosion behavior of the obtained CeO_2 NPs co-deposited zinc phosphate coatings were evaluated by scanning electron microscopy (SEM) and atomic force microscopy (AFM), X-ray diffraction spectroscopy (EDS), X-ray diffraction analysis (XRD), Tafel polarization and electrochemical impedance spectroscopy (EIS), respectively.

2. Materials and Methods

In this study, a carbon steel sheet (St12) was used as the substrate. After the preparation of samples from the steel plate (2×20×30 mm^3), they were abraded by sandpapers with grit sizes of 240, 400, and 600, respectively. The plates were then degreased with acetone and rinsed with distilled water.

The phosphating solution contained phosphoric acid, nitric acid, zinc oxide, and CeO_2 NPs; the quantities of these compounds are presented in Table 1.

Table 1. The chemical composition of the phosphating bath

Compound name	Concentration in the bath
Phosphoric acid (85%) (mL/L)	20
Nitric acid (65%) (mL/L)	22
Zinc oxide (g/L)	15
Nano-CeO_2 g/L	0-0.04-0.07-0.1

Cerium Oxide nanopowder (Sigma Aldrich, 99.95%, < 60 nm) was added to the phosphating baths as the environment-friendly accelerator. Figure 1 shows the field emission-scanning electron microscopy (FE-SEM) image of CeO_2 nanopowder, with a particle size of 30-40 nm.

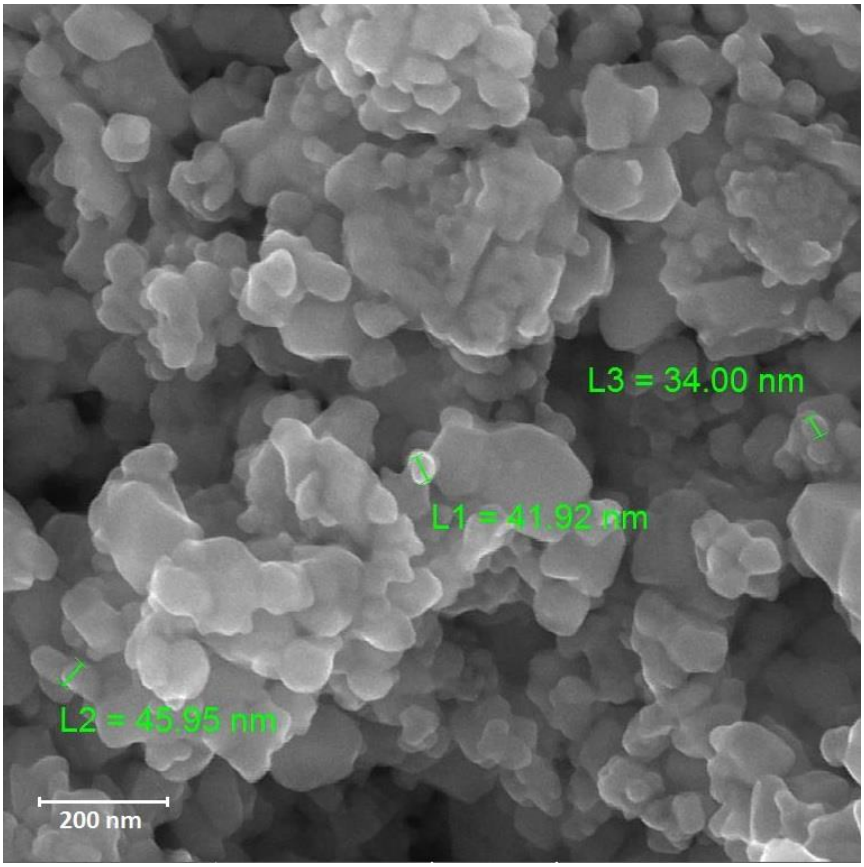

Fig. 1. The FE-SEM image of CeO_2 nanopowder

An ultrasound mixer was employed to disperse the CeO_2 nanopowder in the solution, using a heater, a temperature of 50 °C was reached. Afterward, the samples were immersed in the phosphating solution at 45±5 °C for two minutes.

The zeta potential of nanopowder in the phosphating solution was measured using a Zetasizer 3000Hs system (Malvern, England).

The coating weight per unit area (W) was calculated using the following equation [35]:

$$W=(w_1-w_2)/S \quad (1)$$

where, w_1 and w_2 are the weight of the sample after phosphating and after eliminating the coating, respectively. S is the sample's surface area.

The coating microstructure was studied by SEM (Vega-3 LMU, Tescan). Also, to accurately investigate the microstructure of CeO_2 NPs, SEM (MIRA3, Tescan) was applied. The atomic force microscopy (AFM) images were also prepared using a USPM unit (Ambios, USA).

X-ray diffraction spectroscopy (EDS) was performed using a RONTXT device to determine the percentage of different elements in the coating. The X-ray diffraction (XRD) analysis was also utilized for characterizing the crystal structure of the coatings using a Phillips device (40 kV and 30 mA). Cu-Kα X-ray was used at a wavelength of 1.540598 A° in all experiments. The crystal size of phosphate coatings was calculated using the Scherrer equation [36]:

$$\tau = \frac{K\lambda}{\beta\cos\theta} \quad (2)$$

In this equation, K represents a dimensionless shape factor (0.9), τ represents the crystal size, λ denotes the X-ray wavelength, β is the full-width at half-maximum, and θ is the Bragg angle.

Electrochemical impedance spectroscopy (EIS) and Tafel polarization test were performed to evaluate the corrosion behavior of coatings using a potentiostat (Parstat 2273A). A three-electrode system was used as the test cell, consisting of an Ag/AgCl as the reference electrode, stainless steel as the auxiliary electrode, and the coated samples with an exposed surface of 1 cm^2 as the working electrode. The range of selectable potential in the Tafel test was -250 to 500 mV versus the open circuit potential (OCP), and the scan rate was 0.001 v/s. The experiments were carried out at ambient temperature. PowerCorr software (Ver. 2.47) was applied to evaluate the electrochemical parameters, according to the Tafel extrapolation method. EIS tests were performed at an amplitude of 10 mV versus OCP (E_{Corr}) in the frequency range of 10 mHz to 100 kHz. The polarization resistance (R_p) and double-layer capacitance (C_{dl}) were modeled and calculated by the IviumSoft software (Ver. 2.161) program. This software calculates the best fitting set of parameters with the Levenberg-Marquardt technique between the selected model and the experimental results.

The porosity percentage of phosphate coatings were calculated according to Eq. 3 [37].

$$\varphi = \left(\frac{R_P^{\circ}}{R_P}\right) \times 10^{-\left(\frac{\Delta E_{Corr}}{\beta_a}\right)} \times 100 \quad (3)$$

In these equations, φ represents the porosity percentage, R_P° denotes the polarization resistance of carbon steel substrate in ohm (Ω), $R_{.P.}$ represents the polarization resistance of the sample after phosphating in ohm (Ω), ΔE_{Corr} is the difference in the corrosion potential of base metal before and after applying the coating in volt (V), and β_a represents the anodic Tafel slope of the carbon steel polarization diagram in V/decade.

3. Results and Discussion

3.1. Zeta potential measurements

As mentioned previously, CeO_2 NPs were used as phosphating bath accelerators. Given its accelerating mechanism, which will be explained in the future, CeO_2 NPs were co-deposited with the phosphate crystals. Therefore, the obtained coatings are the composite coatings in which CeO_2 NPs are distributed on the matrix of the phosphate coating. Dispersion of CeO_2 NPs in the phosphating solution for receiving the uniform CeO_2-distributed coatings is a major challenge, as accumulation and deposition of N.P.s in the phosphating solution make preparing the desired coatings complicated. The dispersion properties of CeO_2 NPs were determined by measuring their zeta potential. The mean zeta potential of CeO_2 NPs in the phosphating solution was 24.3 mV in this study. According to Table 2, the N.P.s had primary stability [38]. Consequently, ultrasonic waves were used to disperse CeO_2 NPs in the phosphating solution, which was uniformly precipitated on the coating after homogenization.

Table 2. The relationship between particle stability and zeta potential [37]

Zeta potential (mV)	Particles stability behavior
0 - ±5	Rapid massification
±5 - ±30	Primary stability
±30 - ±40	Moderate stability
±40 - ±60	Good stability
> ±61	Excellent stability

3.2. Weight of phosphate coatings

Figure 2 shows the weight of phosphate coatings as a function of CeO_2 NPs content in the phosphating baths. As seen in Figure 2, a higher coating weight was obtained in the case of CeO_2 NPs incorporated coatings compared to the typical phosphate coating. On the other hand, the weight of phosphate coatings firstly increased with CeO_2 NPs content in the bath from 0 to 0.07 g/L and then decreased. For the amount of N.P.s greater than 0.07 g/L, the agglomeration of nanopowder occurred on the surface, as shown in Figure 3(b), which decreased the coating growth and its weight.

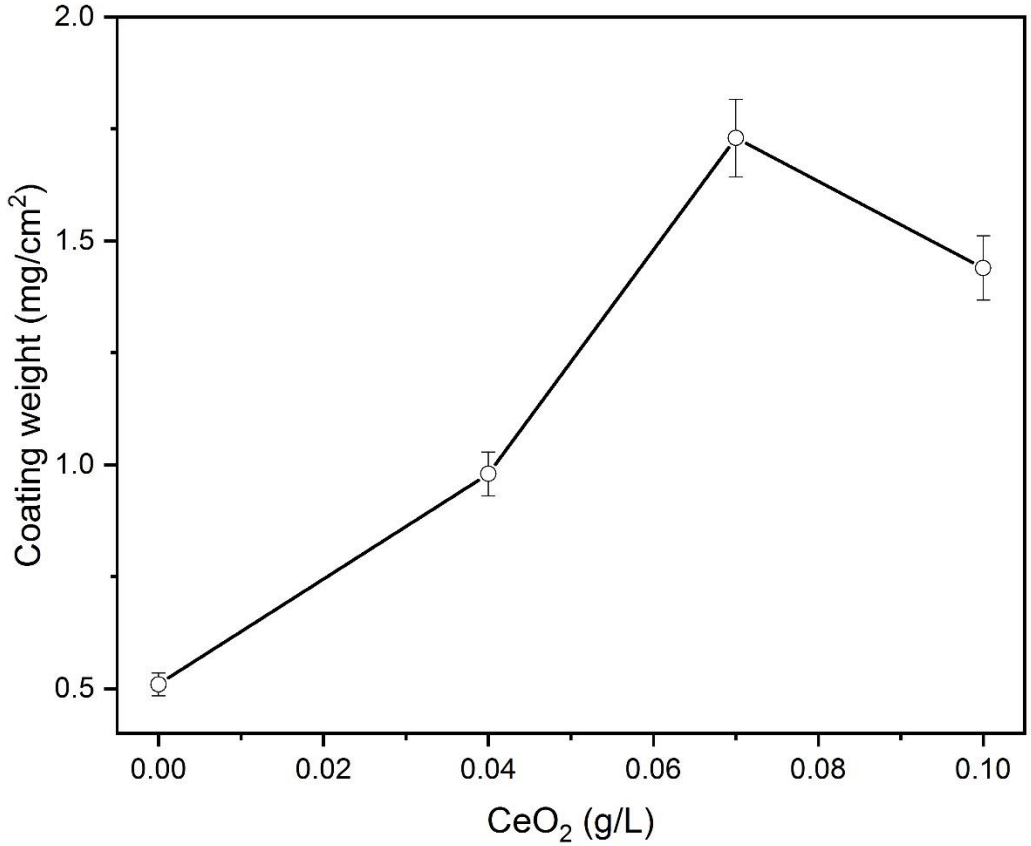

Fig. 2. The weight of phosphate coatings as a function of CeO_2 NPs content in the phosphating baths

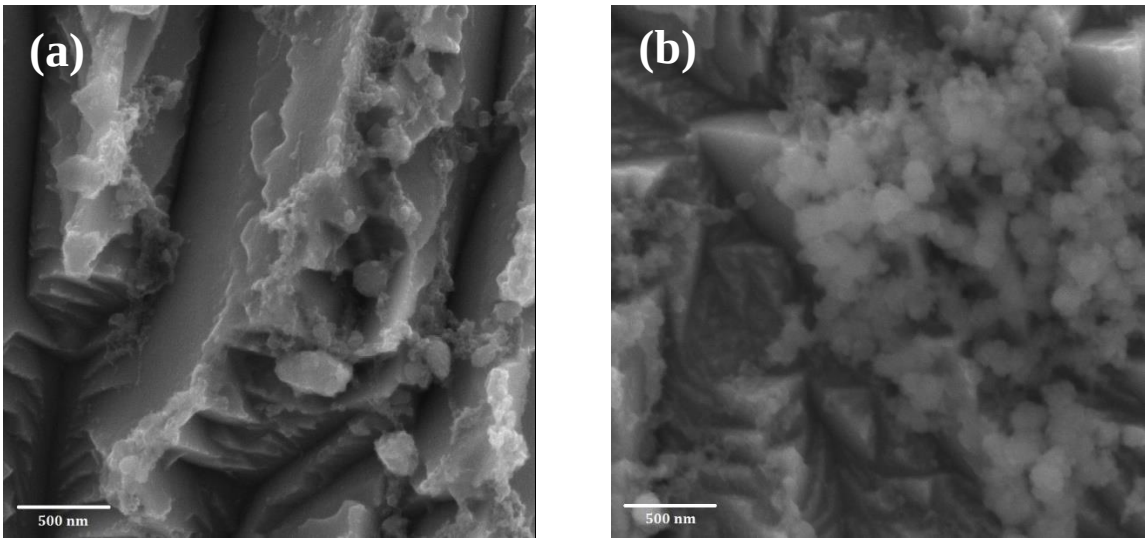

Fig. 3. The distribution of NPs on the coating surface for the amount of NPs (a) 0.04 (b) 0.1 g/L

3.3. Morphological studies

Figure 4 presents the SEM image of phosphate samples in baths containing different quantities of CeO_2 NPs. According to the images, all coatings were well crystallized. The structure of the typical phosphate coating consisted of coarse and non-uniform crystals and was mainly composed of elongated and needle-like crystals and did not produce good coverage due to the low density of crystal clusters. As shown by arrows, because of the low density of the coating crystals and its vertical growth, the covering effect of the coating is not suitable as it was not able to cover a significant portion of the surface area.

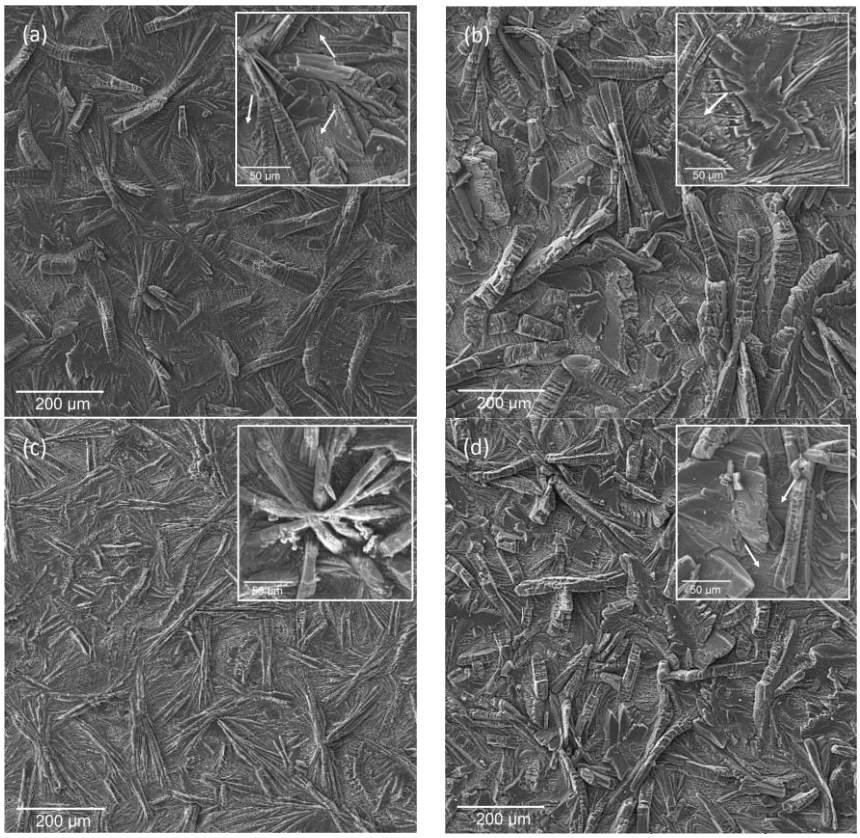

Fig. 4. The SEM images of phosphate samples in baths containing: (a) 0; (b) 0.04; (c) 0.07; and (d) 0.1 g/L of CeO_2 NPs

As presented in Figure 4, the surface density of crystal clusters in samples with the additive was higher than that of phosphate samples in the additive-free bath. The addition of 0.07 g/L of CeO_2 nanopowder to the phosphating bath decreased the coating porosity. It can be related to the more crystal nucleation of the coating due to the presence of CeO_2 NPs.

When the steel substrate is exposed in the phosphating bath, including phosphoric acid, the present equilibrium at the metal/solution interface is disrupted, resulting in more proton consumption and increased pH at the interface. The increase in the pH causes the iron phosphate precipitances to be produced according to the following equation [39]:

$$2H_3PO_4 + Fe \rightarrow Fe(H_2PO_4)_2 + H_2\uparrow \quad (4)$$

On the other hand, while preparing the zinc phosphating solution, the primary zinc phosphate, which is soluble in the solution, forms due to the reaction that occurred between zinc oxide and phosphoric acid, as shown below:

$$ZnO + 2H_3PO_4 \rightarrow Zn(H_2PO_4)_2 + H_2O \quad (5)$$

Then, the formation of zinc-iron phosphate (phosphophyllite) is occurred by performing the reaction between iron phosphate and primary zinc phosphate, according to Eq. (6) [40].

$$2Zn(H_2PO_4)_2 + Fe(H_2PO_4)_2 + 4H_2O \rightarrow Zn_2Fe(PO_4)_2.4H_2O + 4H_3PO_4 \quad (6)$$

Because of the rapid growth of crystal during the process, pH will increase quickly in such a way that the primary phosphate can convert to the insoluble tertiary zinc phosphate (hopeite), according to Eq. (7):

$$3ZnHPO_4 + 4H_2O \Leftrightarrow Zn_3(PO_4)_2.4H_2O + H_3PO_4 \quad (7)$$

It has been shown that CeO_2 NPs were used as an eco-friendly heterogeneous catalyst alone or in association with the other catalysts as Ni to the hydrogen production process [41, 42]. These N.P.s, due to their surface charges, can be easily deposited on the metallic substrate surface. The N.P.s which were physically adsorbed on the surface can provide sites, known as the cathodic region, for hydrogen evolution [19, 22, 43]. The more adsorbed the particles are, the more the hydrogen evaluation will be. Expanding the cathodic region via the increase in the number of adsorbed particles on the surface causes an increase in the number of phosphate crystal nuclei and, as a result, decreases the crystal size of the phosphate coating [44]. Besides, deposited crystals provided nucleation sites for subsequent

coating. Because the evolution rate of hydrogen is much higher when the carbon steel substrate is treated in a phosphate solution with CeO_2 NPs compared to the phosphate solution without N.P.s, at the same thickness, the covering effect of the CeO_2 NPs co-incorporation phosphate coating, particularly the sample with 0.07 g/L CeO_2 NPs, was much better than the traditional phosphate coating. According to Figure 4(c), the coating containing 0.07 g/L of CeO_2 NPs was the most uniform and dense coating among all synthesized coatings.

By adding CeO_2 NPs to the phosphating bath more than the optimal level (0.07 g/L), the coating surface density and uniformity were reduced. Moreover, the phosphate coating containing 0.1 g/L of the additive was not dense and did not show proper coverage of the steel surface (Figure 4(d)). As mentioned before, this finding can be attributed to the higher amount of accumulated CeO_2 NPs in the phosphating solution and its agglomeration on the substrate surface, which occupied the surface anodic sites and consequently prevented anodic reactions [43].

3.4. XRD results

The X-ray diffractograms of phosphate coatings containing CeO_2 NPs, as well as free-CeO_2 coatings, are presented in Figure 5. The results showed that phosphate coatings in baths with and without CeO_2 NPs mainly consisted of iron (0696-006-00), hopeite (0080-039-00), and phosphophyllite (01-083-1246) phases. The iron phase was visible through the carbon steel substrate. The hopeite and phosphophyllite phases were formed on the surface of carbon steel in the zinc phosphate bath [45].

As shown in the figure, the addition of CeO_2 NPs decreased the intensity of the background iron peak. This indicates an increase in the growth and coverage of phosphate crystal clusters in the presence of CeO_2 NPs. The X-ray diffractograms of the coating after the addition of CeO_2 NPs to the phosphating bath were significantly different from the patterns of coating from the additive-free bath. Based on the findings, with the addition of CeO_2 nanopowder to the phosphate coating, the peaks of hopeite and phosphophyllite increased; noting Figure 2, this suggests that a thicker phosphate coating was produced by the addition of CeO_2 NPs to the phosphating bath. As seen in Figure 5, due to the presence of CeO_2 NPs in the phosphating bath, the intensities of phosphophyllite peaks increased more than the hopeite phase. It was shown by Eidivandi et al. [5] that the increase in the phosphophyllite peaks is a result of more surface activation. As seen before, due to the expansion of the sites in the presence of CeO_2 NPs, iron tends to corrode more than in the absence of N.P.s. Therefore, it is logical to accept that the phosphophyllite crystals form the sub-layer on the substrate surface, and then, both the phosphophyllite phase itself and the hopeite phase can grow as a top-layer. The surface agglomerating of N.P.s in the coatings with more than 0.07 g/L CeO_2 NPs prevented the coating crystal growth and weakened both phosphophyllite and hopeite peaks in comparison with the coating, which had the optimum N.P.s content.

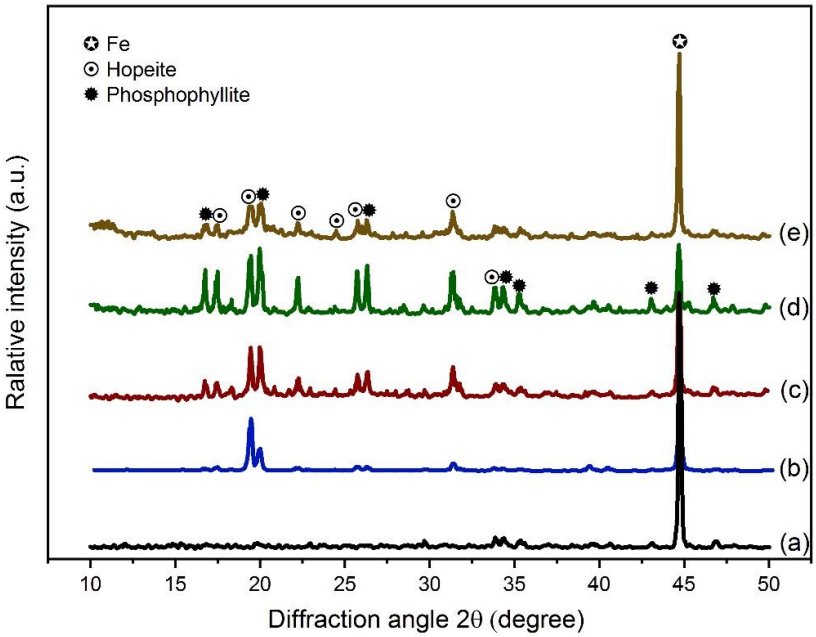

Fig. 5. The X-ray diffractograms of (a) carbon steel substrate and phosphate samples in baths containing: (b) 0; (c) 0.04; (d) 0.07; and (e) 0.1 g/L of CeO_2 NPs

As described before, two main phases of the phosphate coatings, hopeite, and phosphophyllite, were characterized by analyzing the X-ray diffractograms. The peaks observed on 19.408º and 19.991º are the phase main peaks and correspond to the hopeite (Zinc Phosphate Hydrate, $Zn_3(PO_4)_2.4H_2O$) plane of (101) and phosphophyllite (Iron Zinc Phosphate Hydrate, $Zn_2Fe(PO_4)_2.4H_2O$) plane of (111), respectively. The crystal size of both hopeite and phosphophyllite phases of the phosphate coatings in baths with and without CeO_2 NPs was calculated by the Scherrer equation and the main peak data of each phase; the results are presented in Table 3. As can be seen, by adding CeO_2 NPs, the size of both phases crystal decreased. Therefore, it can be said that the presence of CeO_2 NPs by reduction of the nucleation activation energy effectively increased not only the number of cathodic regions but also the number of primary crystals and consequently increased phosphate coating deposition. The results of XRD analysis are consistent with the microstructure observations of phosphate coatings without the additive or with the optimal amount of the additive.

Table 3. The size of phosphate coating crystals with and without CeO_2 NPs

CeO_2 NPs content (g/L)	Crystal size (nm)	
	Hopeite	Phosphophyllite
0	53	71
0.04	40	53
0.07	34	32
0.1	33	25

3.5. Element analysis and distribution map

In the previous section, there was no peak indicating the presence of CeO_2 in the phosphate coatings. This is probably because of its low concentration, which is below the detection limit of the XRD analysis. For the proper investigation, the EDS elemental analysis of phosphate coatings was performed, and the results are presented in Table 4. The cerium (Ce) element was identified in the phosphate coating from the CeO_2 NPs-containing bath. Phosphate coatings with and without CeO_2 NPs are mainly composed of oxygen, phosphorus, iron, and zinc. It can be observed that the phosphate coating in the CeO_2 NPs-containing bath had a lower iron content than the phosphate coating from the bath without CeO_2 NPs; this may show that the surface coverage increased in the presence of the additive. Also, the amount of phosphorus and zinc elements in the additive-containing phosphate coating was higher, indicating the formation of a uniform and thick coating. It can be seen that by the increase in the concentration of CeO_2 NPs in the bath, the agglomeration tendency increases that cause to decrease in the co-deposition of NPs and phosphate crystals. This can be the reason for the decrease in cerium percentage for the sample of 0.07 compared to the sample of 0.1.

The zinc/phosphorus ratio in phosphate coatings from baths with and without CeO_2 NPs is another significant index, which showed that the amount of hopeite phase in the presence of additive was greater than that of the phosphophyllite phase. Besides, the amount of hopeite phase was higher in the additive-containing coating, compared to the additive-free phosphate coating, given the higher zinc content of the additive-containing coating [24, 43].

Table 4. The EDS elemental analysis of phosphate samples in baths containing different concentrations of CeO2 NPs

Additive amount (%)	O	P	Fe	Zn	Ce	Zn/P
0	26.5	11.4	42.9	19.1	0	1.67
0.04	28.4	13.3	35.4	22.9	0.1	1.72
0.07	25.0	12.8	34.8	26.7	0.8	2.08
0.1	24.6	12.3	38.7	23.9	0.5	1.94

On the other hand, Figure 6 depicts the distribution map of CeO_2 in the phosphate coating. It can be claimed that the ceria had a uniform distribution in the coating. When phosphating reactions occur on the surface, the ceria NPs are trapped between phosphate crystals and form a nano-composite layer on the top of the surface. This fact shows that CeO_2 NPs not only acts as an effective phosphating bath accelerator but also by co-depositing with phosphate crystals, making it a nano-composite phosphate coating. The latter can affect the many properties of the coating, such as its corrosion behavior.

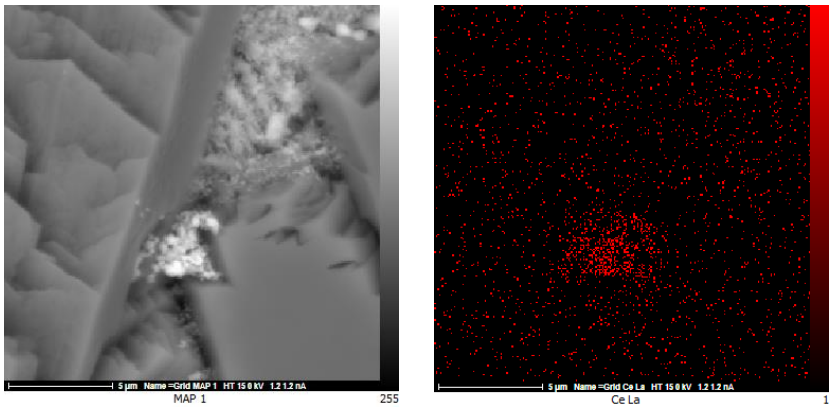

Fig. 6. The distribution map of cerium in the phosphate coating

3.6. Corrosion behavior of coatings

The polarization curves of different coatings are presented in Figure 7. To accurately analyze the results presented in Figure 7, various electrochemical parameters, including the anodic slope (β_a), cathodic slope (β_c), corrosion potential (E_{Corr}), corrosion current density (i_{Corr}), and polarization resistance (R_p), were calculated using the Tafel extrapolation method; the results are indicated in Table 5.

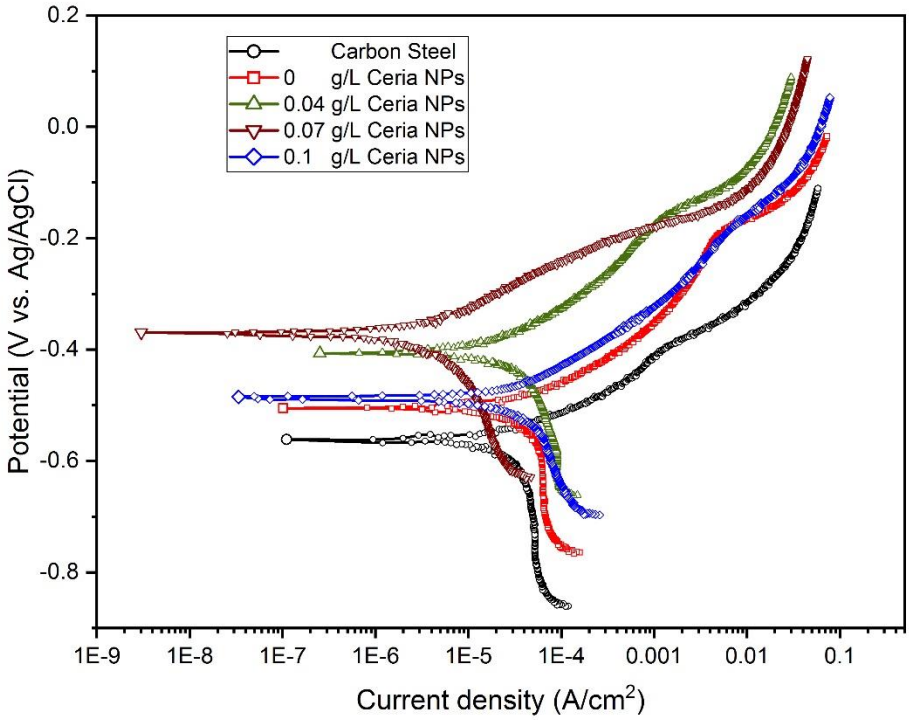

Fig. 7. The polarization curves of steel samples coated in baths containing different amounts of CeO_2 NPs

The results indicate that adding CeO_2 NPs to the phosphating bath decreased the coating corrosion current density (i_{Corr}) as well as shifted the corrosion potential (E_{Corr}) towards less negative values, which is due to increasing the surface resistance of coating against corrosion.

It was explained in section 3.3 that the traditional phosphate coating could not cover the substrate surface areas perfectly (Figure 4(a)) and in the other samples except the phosphate coating with 0.07 g/L CeO_2 NPs, some regions which are generally iron-enriched areas, remained uncoated (Figure 4(b) and (d)). On the other hand, it was shown that the addition of CeO_2 NPs up to 0.07 g/L in the phosphating bath could decrease the iron-enriched surface areas by preparing more coverage of the coatings, which is emphasized by decreasing the intensity of Fe peak in XRD diffractograms (Fig. 5). So, the increase in both corrosion potential and corrosion current density of the coatings relative to the uncoated carbon steel substrate is logical, and it can be attributed to more coverage of the surface by CeO_2 NPs co-incorporated

phosphate coatings as the less iron-enriched the areas are, the less the negative corrosion potentials and the more the corrosion current density of CeO_2 NPs co-incorporated phosphate coatings will be. On the other hand, the magnitude of change in the corrosion potential and corrosion current density is often a function of the weight and porosity of phosphate coatings [5, 19, 24].

Table 5. The electrochemical parameters from the polarization curves for surface-modified steel samples with phosphate coatings containing various quantities of CeO_2 NPs

Additive amount (g/L)	E_{Corr} (V)	i_{Corr} ($\mu A/cm^2$)	β_a (V/dec)	β_c (V/dec)	R_p (Kohm)	Porosity percentage
Carbon Steel	-0.56	16.6	0.054	0.11	986	-
0	-0.5	12.5	0.059	0.11	1429	13.9
0.04	-0.41	10.7	0.091	0.089	1722	3.9
0.07	-0.37	2.2	0.07	0.128	8860	1.7
0.1	-0.49	12.2	0.058	0.074	1320	6.8

In Table 5, the calculated porosity percentage of the different coatings, based on Eq. 3, is also shown. Phosphate coatings are usually porous, which improves color adhesion on the surface. On the other hand, porosity is associated with electrolyte penetration, which results in corrosion. When the corrosive medium penetrates the surface defects, it passes through the crystal layer and reaches the substrate, resulting in an increase in corrosion current density due to reactions with iron [19]. As indicated in Table 5, the traditional phosphate coating has high porosity. As seen in the SEM images (Figure 4), the structure of phosphate coating in the bath without CeO_2 NPs consisted of scattered and elongated crystal clusters with inadequate coverage; this structure was not compacted and contained many pores. By calculating the porosity percentage, the relative plurality of coating-free areas was revealed. However, the porosity of coating was significantly reduced by increasing CeO_2 NPs content as it has a minimum at 0.07 g/L. Reduction in porosity after adding 0.07 g/L of CeO_2 NPs to the phosphating bath can be related to NPs acceleration role to increase in the nucleation rate of phosphate crystals and consequently the increase in coverage. CeO_2 NPs as an accelerator could increase the number of crystal nuclei and speed up the phosphating process rate. As a result, the coating incorporated with CeO_2 NPs, particularly the coating with 0.07 g/L CeO_2 NPs, possesses a dense and uniform coating with the lowest porosity which is required to have excellent corrosion protection. The denser coating has fewer micro-cracks and then holds stronger resistance to the permeability of electrolytes. Besides, the coating with 0.07 g/L CeO_2 NPs also has the maximum weight, which is indicative of the thickest phosphate coating layer. Thus, it is the denser and thicker coating layer of the coating with 0.07 g/L CeO_2 NPs that accounts for its stronger corrosion resistance compared to other specimens. However, after adding larger amounts of the additive (0.1 g/L) to the phosphating bath, the corrosion potential decreased while the corrosion current density increased. The loss of corrosion resistance at higher concentrations of the additive can be attributed to the high amount of CeO_2 NPs in the phosphating solution, which may lead to the accumulation of NPs, halt the accelerating role of CeO_2 NPs, and make the formation of intact phosphate coatings difficult [43]. Consequently, the corrosive medium passes through open porosities, as well as the intersecting crystal boundaries of the phosphate layer. Owing to the corrosive medium reaction with the substrate, the corrosion current density increased, and the potential for corrosion reduced; this can justify the reduction in the anti-corrosion activity and protection efficiency of coating with 0.1 g/L of CeO_2 NPs versus 0.07 g/L of CeO_2 NPs. These results are in complete agreement with the SEM results (Figure 4), as well as the potentiodynamic polarization test results (Figure 7).

For further investigation, electrochemical impedance spectroscopy (EIS) was also performed for carbon steel and phosphate samples in baths containing different concentrations of CeO_2 NPs in 3.5% NaCl solution. Figure 8 shows obtained Nyquist plots, and the inset figures illustrate their corresponding Bode plots and the Randles circuit used for the extraction of impedance data. According to Figure 8, all Nyquist curves contain only one depressed semi-circle, and for all samples, Bode diagrams indicated one time constant; as a result, the EIS results were simulated with the equivalent circuit of Randles. In the equivalent circuit, R_s is the electrolyte resistance, R_t is polarization resistance at the electrolyte/electrode interface, which is the same as charge transfer resistance, and CPE is the phase constant capacitance element. It is generally believed that the CPE originates from the current density distribution on the inhomogeneous electrode surface, like porous electrodes [46]. Because the phosphate coating surfaces are not completely uniform and ideal, the capacitor cannot be used in equivalent circuits, and

therefore, CPE was utilized instead of a capacitor. Constant phase element can be modeled by Eq. (12):

$$Z_{CPE}=\frac{1}{Q*(j\omega)^{n}} \quad (12)$$

where Z_{CPE} is impedance, j is the square root of -1, ω is the frequency and n is the ideality of the capacitor which is 0-1. For many metal or solid electrodes, the measured impedance in the double-layer region (no faradaic current) follows a power law, such as that for the CPE, with a value of n between 0.9 and 1.0. When this element is in parallel with a charge-transfer resistance (Rt), the Nyquist plot is an arc of a circle with the center below the x-axis, as shown in Figure 8 [5, 37]. The obtained value from the fitting of equivalent circuit and spectra including R_p, R_s, and CPE were calculated for carbon steel and the coated samples in baths containing different amounts of the additive; the results are presented in Table 6.

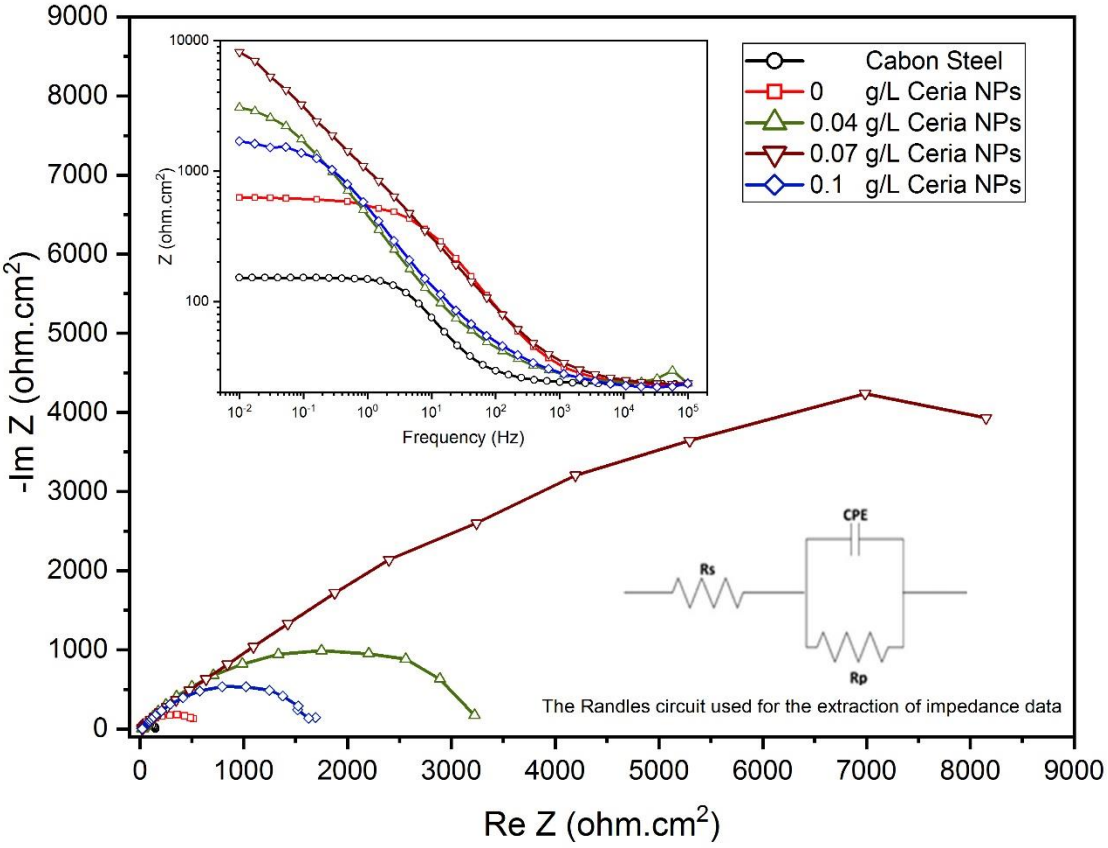

Fig. 8. The Nyquist plots of the EIS test for phosphate samples in baths containing different amounts of CeO_2 NPs

The EIS diagrams of phosphate samples are similar in baths with and without CeO_2 NPs. The increase in the diameter of semicircles indicates an increase in the polarization resistance of coatings. The results showed that phosphate samples had a higher polarization resistance than carbon steel substrate; therefore, phosphate coatings might prevent surface reactions against 3.5% NaCl solution as far as possible.

Table 6. The EIS data for surface-modified steel samples with phosphate coatings containing various quantities of CeO_2 NPs

Additive amount (g/L)	R_s ($\Omega.cm^2$)	R_p ($\Omega.cm^2$)	CPE ($\Omega^{-1}.cm^{-2}.S^n$)
Carbon Steel	26	128.8	80×10^{-6}
0	23	578.7	2.48×10^{-6}
0.04	25	3300	9.5×10^{-6}
0.07	25	15970	0.99×10^{-6}
0.1	22	1760	10.54×10^{-6}

As illustrated in the Nyquist plots and Table 6, polarization resistance increased by adding 0.04 g/L of CeO_2 NPs to the phosphating bath. The polarization resistance improved again by increasing the amount of additive to 0.07 g/L. However, when the concentration of CeO_2 NPs exceeded 0.07 g/L (0.1 g/L), the polarization resistance decreased, which is indicative of a reduction in corrosion protection. Since most electrochemical corrosion attacks occur on the surface of phosphate coatings, reactants and corrosion products should be transmitted during the corrosion process. Based on the findings, reaction resistance increases by increasing the thickness of the protective layer [25, 43].

The results of multiple tests showed that the addition of CeO_2 NPs to the phosphating bath produced denser and thicker coatings with better coverage and lower porosity compared to typical phosphate coatings. Therefore, coatings containing the additive exhibited higher corrosion resistance than phosphate coatings without the additive. Among additive-containing coatings, the phosphate sample had the highest polarization resistance in the presence of 0.07 g/L of CeO_2 NPs, which represents the optimal amount of the additive. However, the addition of CeO_2 NPs to the phosphating bath more than the optimal amount resulted in a decline in polarization resistance due to inadequate coverage and lower density; these results are in agreement with the morphological study of coatings (Figure 4).

4. Conclusion

In the present study, the addition of CeO_2 nanopowder to zinc phosphate coating was found to be useful in accelerating the phosphating process. The EDS and SEM analyses showed that CeO_2 NPs could act as a nucleating agent and reduce the size of crystals while increasing the coating coverage (dense coating). The coatings were mainly composed of hopeite and phosphophyllite phases. The optimal amount of the additive in the phosphatizing bath was determined to be 0.07 g/L. Based on the findings, the phosphatized coatings in the bath containing the optimal amount of the additive showed the lowest porosity; this might result from an increase in the cathodic region for deposition of the coating. The results of polarization and EIS tests showed that the optimal amount of the additive could significantly improve the corrosion resistance of phosphate coatings. However, when the amount of CeO_2 NPs increased to more than the optimal level, corrosion resistance reduced due to the accumulation of NPs and defective phosphate coatings.

References

[1] L. Niu, R. Guo, C. Tang, H. Guo, J. Chen, "Surface characterization and corrosion resistance of fluoferrite conversion coating on carbon steel" Surface and Coatings Technology, Vol. 300, 2016, pp. 110.

[2] C.-c. Jiang, Y.-k. Cao, G.-y. Xiao, R.-f. Zhu, Y.-p. Lu, "A review on the application of inorganic nanoparticles in chemical surface coatings on metallic substrates" RSC advances, Vol. 7, 2017, pp. 7531.

[3] O. Girčienė, R. Ramanauskas, L. Gudavičiūtė, A. Martušienė, "The effect of phosphate coatings on carbon steel protection from corrosion in a chloride-contaminated alkaline solution" J. of CHEMIJA, Vol. 24, 2013, pp. 251.

[4] B. Ramezanzadeh, M. Akbarian, M. Ramezanzadeh, M. Mahdavian, E. Alibakhshi, P. Kardar, "Corrosion protection of steel with zinc phosphate conversion coating and post-treatment by hybrid organic-inorganic sol-gel based silane film" Journal of The Electrochemical Society, Vol. 164, 2017, pp. C224.

[5] S. Eidivandi, B.S. Boroujeny, A. Dustmohammadi, E. Akbari, "The effect of surface mechanical attrition treatment (SMAT) time on the crystal structure and electrochemical behavior of phosphate coatings" Journal of Alloys and Compounds, Vol. 821, 2020, pp. 153252.

[6] C. Galvan-Reyes, J. Fuentes-Aceituno, A. Salinas-Rodríguez, "The role of alkalizing agent on the manganese phosphating of a high strength steel part 1: The individual effect of NaOH and NH4OH" Surface and Coatings Technology, Vol. 291, 2016, pp. 179.

[7] B. Ramezanzadeh, H. Vakili, R. Amini, "The effects of addition of poly (vinyl) alcohol (PVA) as a green corrosion inhibitor to the phosphate conversion coating on the anticorrosion and adhesion properties of the epoxy coating on the steel substrate" Applied Surface Science, Vol. 327, 2015, pp. 174.

[8] M. Morks, P. Corrigan, N. Birbilis, I. Cole, "A green MnMgZn phosphate coating for steel pipelines transporting CO2 rich fluids" Surface and Coatings Technology, Vol. 210, 2012, pp. 183.

[9] M. Farias, C. Santos, Z. Panossian, A. Sinatora, "Friction behavior of lubricated zinc phosphate coatings" Wear, Vol. 266, 2009, pp. 873.

[10] G. Parker, Encyclopedia of materials: science and technology, 2001.

[11] N. Bay, Metal forming and lubrication, Encyclopedia of Materials: Science and Technology, Elsevier2000, pp. 5377-5380.

[12] M. Fouladi, A. Amadeh, "Effect of phosphating time and temperature on microstructure and

corrosion behavior of magnesium phosphate coating" Electrochimica Acta, Vol. 106, 2013, pp. 1.
[13] J. Popić, B. Jegdić, J. Bajat, Đ. Veljović, S. Stevanović, V. Mišković-Stanković, "The effect of deposition temperature on the surface coverage and morphology of iron-phosphate coatings on low carbon steel" Applied Surface Science, Vol. 257, 2011, pp. 10855.
[14] A. Valanezhad, K. Tsuru, M. Maruta, G. Kawachi, S. Matsuya, K. Ishikawa, "Zinc phosphate coating on 316L-type stainless steel using hydrothermal treatment" Surface and Coatings Technology, Vol. 205, 2010, pp. 2538.
[15] S. Jegannathan, T.S. Narayanan, K. Ravichandran, S. Rajeswari, "Formation of zinc phosphate coating by anodic electrochemical treatment" Surface and Coatings Technology, Vol. 200, 2006, pp. 6014.
[16] B.-i. LIN, J.-T. Lu, K. Gang, L. Jun, "Growth and corrosion resistance of molybdate modified zinc phosphate conversion coatings on hot-dip galvanized steel" Transactions of Nonferrous Metals Society of China, Vol. 17, 2007, pp. 755.
[17] T.S. Narayanan, S. Jegannathan, K. Ravichandran, "Corrosion resistance of phosphate coatings obtained by cathodic electrochemical treatment: Role of anode–graphite versus steel" Progress in organic coatings, Vol. 55, 2006, pp. 355.
[18] G. Li, L. Niu, J. Lian, Z. Jiang, "A black phosphate coating for C1008 steel" Surface and Coatings Technology, Vol. 176, 2004, pp. 215.
[19] M. Sheng, Y. Wang, Q. Zhong, H. Wu, Q. Zhou, H. Lin, "The effects of nano-SiO2 additive on the zinc phosphating of carbon steel" Surface and Coatings Technology, Vol. 205, 2011, pp. 3455.
[20] F. Fang, J.-h. Jiang, S.-Y. Tan, A.-b. Ma, J.-q. Jiang, "Characteristics of a fast low-temperature zinc phosphating coating accelerated by an ECO-friendly hydroxylamine sulfate" Surface and Coatings Technology, Vol. 204, 2010, pp. 2381.
[21] Y. Tian, W. Qiu, Y. Xie, H. Huang, J. Hu, L. Zhong, X. Jiang, X. Zhang, "Melatonin as an accelerating agent for phosphate chemical conversion coatings on mild steel with enhanced corrosion resistance" Journal of the Electrochemical Society, Vol., 2020, pp.
[22] C.-c. Jiang, R.-f. Zhu, G.-y. Xiao, Y.-z. Zheng, L.-l. Wang, Y.-p. Lu, "Effect of nano-SiO2 particles and sol on phosphate conversion coatings on 35CrMnSi steel" Journal of The Electrochemical Society, Vol. 163, 2016, pp. C571.
[23] X. Tan, F. Nan, Performance of Modified Nano-SiO2 Composite Phosphating Coating on the Surface of Steel, IOP Conference Series: Materials Science and Engineering, IOP Publishing, 2020, p. 012002.
[24] M. Tamilselvi, P. Kamaraj, M. Arthanareeswari, S. Devikala, J.A. Selvi, "Development of nano SiO2 incorporated nano zinc phosphate coatings on mild steel" Applied Surface Science, Vol. 332, 2015, pp. 12.
[25] S. Shibli, F. Chacko, "Development of nano TiO2-incorporated phosphate coatings on hot dip zinc surface for good paintability and corrosion resistance" Applied Surface Science, Vol. 257, 2011, pp. 3111.
[26] K. Mašek, J. Beran, V. Matolín, "RHEED study of the growth of cerium oxide on Cu (1 1 1)" Applied Surface Science, Vol. 259, 2012, pp. 34.
[27] T. Montini, M. Melchionna, M. Monai, P. Fornasiero, "Fundamentals and catalytic applications of CeO2-based materials" Chemical reviews, Vol. 116, 2016, pp. 5987.
[28] B.C. Nelson, M.E. Johnson, M.L. Walker, K.R. Riley, C.M. Sims, "Antioxidant cerium oxide nanoparticles in biology and medicine" Antioxidants, Vol. 5, 2016, pp. 15.
[29] C. Walkey, S. Das, S. Seal, J. Erlichman, K. Heckman, L. Ghibelli, E. Traversa, J.F. McGinnis, W.T. Self, "Catalytic properties and biomedical applications of cerium oxide nanoparticles" Environmental Science: Nano, Vol. 2, 2015, pp. 33.
[30] K.A. Ledwa, L. Kępiński, "Dispersion of ceria nanoparticles on γ-alumina surface functionalized using long chain carboxylic acids" Applied Surface Science, Vol. 400, 2017, pp. 212.
[31] S. Ranganatha, T. Venkatesha, K. Vathsala, "Electrochemical studies on Zn/nano-CeO2 electrodeposited composite coatings" Surface and Coatings Technology, Vol. 208, 2012, pp. 64.
[32] J. Huiming, S. Jiang, L. Zhang, "Structural characterization and corrosive property of Ni-P/CeO2 composite coating" Journal of Rare Earths, Vol. 27, 2009, pp. 109.
[33] W.-c. Sun, J.-M. Xu, Y. Wang, F. Guo, Z.-W. Jia, "Effect of Cerium Oxide on Morphologies and Electrochemical Properties of Ni-WP Coating on AZ91D Magnesium" Journal of Materials Engineering and Performance, Vol. 26, 2017, pp. 5753.
[34] L. Ecco, M. Fedel, A. Ahniyaz, F. Deflorian, "Influence of polyaniline and cerium oxide nanoparticles on the corrosion protection properties of alkyd coating" Progress in Organic Coatings, Vol. 77, 2014, pp. 2031.
[35] E. Banczek, P. Rodrigues, I. Costa, "The effects of niobium and nickel on the corrosion resistance of the zinc phosphate layers" Surface and Coatings Technology, Vol. 202, 2008, pp.
[36] N. Rezaee, M. Attar, B. Ramezanzadeh, "Studying corrosion performance, microstructure and

adhesion properties of a room temperature zinc phosphate conversion coating containing Mn2+ on mild steel" Surface and Coatings Technology, Vol. 236, 2013, pp. 361.
[37] F. Saberi, B.S. Boroujeny, A. Doostmohamdi, A.R. Baboukani, M. Asadikiya, "Electrophoretic deposition kinetics and properties of ZrO2 nano coatings" Materials Chemistry and Physics, Vol. 213, 2018, pp. 444.
[38] A. Standard, "Zeta potential of colloids in water and waste water" ASTM Standard D, Vol., 1985, pp. 4187.
[39] A. KozŁowski, "Dry friction of manganese phosphate coatings on steel and cast iron" Electrodeposition and Surface Treatment, Vol. 2, 1974, pp. 109.
[40] K. Chandrasekaran, S.N. TS Nellaiappan, R. Kulandaivelu, M.H. Lee, "Improving the reactivity and receptivity of alloy and tool steels for phosphate conversion coatings: role of surface mechanical attrition treatment" Industrial & Engineering Chemistry Research, Vol. 53, 2014, pp. 20124.
[41] L. Qihai, L. Zili, Z. Xinhua, L. Cuijin, D. Jiao, "Hydrogen production by steam reforming of ethanol over copper doped Ni/CeO2 catalysts" Journal of Rare Earths, Vol. 29, 2011, pp. 872.
[42] R. Pérez-Hernández, Catalytic Ni/CeO 2 Nanorods and Ag/CeO 2 Nanotubes for Hydrogen Production by Methanol Reforming, Advanced Catalytic Materials: Current Status and Future Progress, Springer2019, pp. 167-190.
[43] M. Tamilselvi, P. Kamaraj, M. Arthanareeswari, S. Devikala, "Nano zinc phosphate coatings for enhanced corrosion resistance of mild steel" Applied Surface Science, Vol. 327, 2015, pp. 218.
[44] M. Manna, A. Shah, S. Kulkarni, "Development of phosphate coating on the surface of TMT rebar: an option to study the effect of n-SiO2 as an additive" Ironmaking & Steelmaking, Vol. 44, 2017, pp. 666.
[45] D.B. Freeman, phosphating and metal pre-treatment: a guide to modern processes and practice, Woodhead-Faulkner, Cambridge, 1986.
[46] R. De Levie, "The influence of surface roughness of solid electrodes on electrochemical measurements" Electrochimica Acta, Vol. 10, 1965, pp. 113.